Rendering of Unfalsified PID Gain Sets for Parameter Space Control Design

Masami Saeki
Department of Mechanical System Engineering, Hiroshima University
Kagamiyama 1-4-1 Higashi-Hiroshima, Japan 739–8527
Email: saeki@hiroshima-u.ac.jp

***Abstract*—In this paper, a new approach to the data-driven PID control design in parameter space is proposed. Namely, first, volume data of the PID gains that are falsified by a necessary condition for the maximum sensitivity constraint is calculated, and next it is visualized by volume rendering. Because of the recent development of parallel computation and GPU(graphics processing unit), rendering can be easily applied, and our main issue is how fast the volume data can be calculated by the parallel computation. We give an estimation method of the ℓ_2 gain using a filter bank from a finite length response data, and this method is used for the volume data calculation at ten-thousand grid points. Efficiency and accuracy of our algorithm are examined by numerical experiments.**

I. INTRODUCTION

PID control is widely used for many industrial plants, and it is important to set the PID gain at the appropriate value for energy saving and high-quality products. However, it is said that half of the PID gains are not well-tuned. In model-based control design, plant modeling is usually costly or modeling error brings about inherent difficulty. It is expected that a data-driven design method that does not require plant modeling has the potential to give a solution to this problem. Several data driven design methods have been proposed [1]-[6].

Loop shaping is recognized as a useful and primary design criterion in the robust control design [8]. We have proposed a data-driven loop shaping design method for PID control based on the unfalsified control concept of [9], [10]. We have developed a parameter plane method [5] and a numerical optimization method [11], where a problem of maximizing the integral gain of the PID controller subject to the maximum sensitivity constraint or the open-loop stability constraint is considered. The former constraint is non-convex, and a local solution is searched for by optimization. The latter constraint is linear, and the global solution is obtained but it is only applicable to stable plants.

These our methods have the following features. First, one-shot plant response data that may be measured in the normal operating condition can be used for design, if the plant is sufficiently excited at the steady state and the influence of the disturbance to the response data is negligibly small during the experimental phase for the tuning of the controllers. Second, many fictitious plant responses are generated by filtering the one-shot plant response with many bandpass filters, i.e. a filter bank. This filter bank method is essential for the improvement of the efficiency of controller falsification. Third, in the design methods based on model matching such as VRFT[7], it is difficult to find an adequate reference model especially for those plants with time-delay and/or unstable-zeros[7]. It is shown by numerical examples that appropriate PID gains can be obtained by our method even for those plants without identification of the time-delay and unstable zeros[6], [11].

It is interesting and useful to visualize the unfalsified set in the 3D (dimensional) space and to understand the relation between the set and the solutions obtained by the optimization method. However, our parameter plane method is not satisfactory for this purpose. Namely, every time γ level, which gives the maximum sensitivity bound, is given, many ovals that correspond to the sample frequencies are drawn on the parameter plane (K_P, K_I) as shown in Fig. 1. Since the points inside the ovals are falsified, the boundary of the unfalsified set is given by an envelope curve of the ovals. Namely the unfalsified set shown by the shaded area is not directly drawn, and hence special knowledge is necessary to find the unfalsified set. The set in the 3D parameter space is displayed only by drawing the cross-section of the set on the planes (K_P, K_I) or (K_P, K_D). A new method by which the unfalsified set can be visualized in the 3D space is necessary.

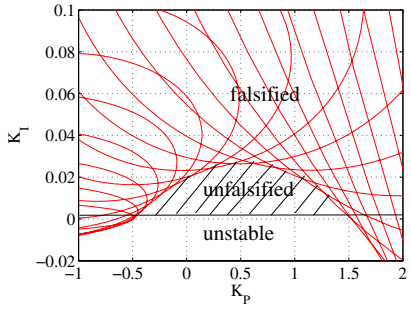

Fig. 1. Parameter plane method

In this paper, we will propose a visualization method of the unfalsified set in the 3D space by volume rendering. Volume rendering has been applied to MRI data, flow simulation data, and so on, and the graphical representation can be rotated freely, and the shape can be deformed continuously by this method. In the literature of parameter space approach [12], permissible regions are calculated exactly for control design for mathematical plant models, and the sets are drawn on the 2D plane in most cases. There has been no study about the application of the volume rendering to a parameter space design as far as the author knows. The main issue of this method is the fast calculation of the volume data.

978-1-4673-5769-2/13/$31.00 ©2013 IEEE

In Section 2, we explain about the volume data briefly, and give the problem setting in Section 3. In Section 4, an ℓ_2 gain estimation method using a filter bank is explained, and, an ℓ_2 gain estimation method based on the extension theorem is also explained for comparison. Further, a method of visualizing the intersection of two unfalsified sets is proposed. In Section 5, computation time by these two methods are compared with each other, and in Section 6, the design method is demonstrated for a boiler benchmark problem[16].

The following notations will be used. The z transform of a sequence $x = \{x_i,\ i = 0, 1, 2, 3, \cdots\}$ is represented by $x(z)$. π_q denotes the q step truncation operator, namely, $\pi_q x = \{x_i,\ i = 0, 1, 2, \cdots, q-1\}$. The column vector corresponding to the sequence $\pi_q x$ is denoted by $\hat{x}_q$, namely, $\hat{x}_q = (x_0, x_1, \cdots, x_{q-1})^T$. The ℓ_2-norm of a sequence x is denoted by $\|x\|_2$. Therefore,

$$\|x\|_2 = \sqrt{\sum_{i=0}^{\infty} x_i^2}, \quad \|\pi_q x\|_2 = \sqrt{\sum_{i=0}^{q-1} x_i^2} \tag{1}$$

II. A NEW PARAMETER SPACE METHOD BY VOLUME RENDERING

Volume rendering is the creation of graphical representations of volume data sets that are defined on three-dimensional grids. Volume data sets are characterized by multidimensional arrays of scalar or vector data. These data are typically defined on lattice structures representing values sampled in the 3D space. If a volume data is given, it can be easily visualized by using a software such as MATLAB on a average personal computer with a GPU card.

Therefore, our main issue is how fast a scalar volume data can be calculated. Since our purpose is to visualize the surface composed of the PID gains that give the same maximum sensitivity, the volume data is a list of the estimated values of the maximum sensitivity at the grid points as shown in Fig. 2. Let the parameters K_P, K_I, and K_D be related to the $x,\ y,\ z$ coordinates, respectively, and let the number of the sample points of each axis be $n_x,\ n_y,\ n_z$. Then, the total number of the grid points becomes $n_{\text{total}} = n_x n_y n_z$. For example, $n_{\text{total}} = 8000$ for $n_x = n_y = n_z = 20$.

Since the calculation of the volume data is an off-line data processing, the computation time is not required to be very fast, but shorter is more preferable. Recently, parallel computation using multi-core processors, GPUs, or computer clusters is becoming popular. We will use Parallel Computing Toolbox of MATLAB in the numerical experiments. The calculation for many grid points is suitable for parallel computation, and hence we expect that the computation time will be made much shorter. We will examine two estimation methods of the maximum sensitivity and the effect of parallel computation by numerical examples.

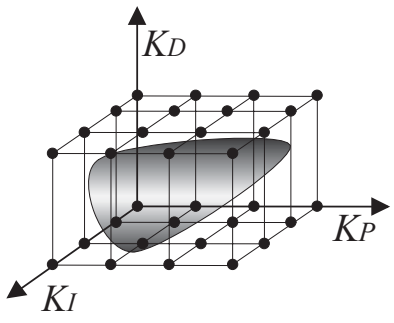

Fig. 2. Grid points for volume data

III. PROBLEM SETTING

Consider a single-input single-output linear time-invariant plant described by

$$y(z) = P(z)u(z) \tag{2}$$

Input and output responses are represented by $u = \{u_i,\ i = 0, 1, 2, 3, \cdots\}$ and $y = \{y_i,\ i = 0, 1, 2, 3, \cdots\}$ with sampling period h[s], respectively.

One shot finite sequence plant responses $\pi_q u$ and $\pi_q y$ are assumed to be available for the calculation, where the plant is at the steady state at $i = 0$. The plant responses can be measured in both open-loop and closed-loop operations, and the disturbance must be very small during the measurement. $P(z)$ is assumed to be unidentified.

We have considered the next feedback system for a loop shaping design.

$$y(z) = P(z)u(z) \tag{3}$$
$$u(z) = -K(z)y(z) + w(z) \tag{4}$$

where $w(z)$ is a disturbance, and $K(z)$ is a PID controller described by

$$K(z) = K_P + K_I \frac{hz^{-1}}{1 - z^{-1}} + K_D \frac{1 - z^{-1}}{h} \tag{5}$$

The PID gain is the design parameter, and represented by a vector $f = [K_P, K_I, K_D]$.

The summation of the plant output for a unit step disturbance $w = \{1,\ i = 0, 1, 2, 3, \cdots\}$ with zero initial condition is given by

$$\sum_{i=0}^{\infty} y_i = \frac{1}{K_I} \tag{6}$$

This is easily derived by using the final value theorem. Therefore, it is expected that the disturbance rejection may be improved by maximizing K_I.

The sensitivity and complementary sensitivity functions are given by

$$S(z) = \frac{1}{1 + P(z)K(z)} \tag{7}$$
$$T(z) = \frac{P(z)K(z)}{1 + P(z)K(z)} \tag{8}$$

Stability margin of the closed-loop system is estimated by the maximum sensitivity. The maximum complementary sensitivity is used as an auxiliary criterion. Thus, the minimization problem of K_I subject to the closed-loop stability and

$$\gamma_S \geq |S(e^{j\omega h})|, \quad \omega_S \in [0, \pi/h] \tag{9}$$
$$\gamma_T \geq |T(e^{j\omega h})|, \quad \omega_T \in [0, \pi/h] \tag{10}$$

can be considered. The continuous time version has been given as MIGO in [13]. We have studied a data-driven version of this problem under the assumption that one-shot plant response data are available instead of $P(z)$. For a fixed frequency ω, the constraint (9) is concave with respect to f, and the constraint $\gamma_T \geq |T(e^{j\omega h})|$ is convex or non-convex depending on the largeness of γ_T.

This problem is described as follows in the parameter space. Define the next two sets for given γ_S-level and γ_T-level.

$$\mathcal{F}_S(\gamma_S) = \left\{ f : \gamma_S \geq \max_{\omega \in [0,\ \pi/h]} |S(e^{j\omega h})| \right\} \tag{11}$$

$$\mathcal{F}_T(\gamma_T) = \left\{ f : \gamma_T \geq \max_{\omega \in [0,\ \pi/h]} |T(e^{j\omega h})| \right\} \tag{12}$$

Then, the minimization problem is a problem of finding a point for which K_I is maximized in the set $\mathcal{F}_S(\gamma_S)$, or the set $\mathcal{F}_S(\gamma_S) \cap \mathcal{F}_T(\gamma_T)$. Therefore, we may consider a problem of visualizing each set and the intersection of the two sets in the parameter space of the PID gain f.

We will estimate the maximum sensitivity for the grid points of PID gains by using a finite length plant response in order to make a volume data. We will apply our previous results of [15]. Note that the maximum sensitivity equals to the ℓ_2 gain of the sensitivity function. From

$$u(z) = S(z)w(z), \tag{13}$$

we obtain

$$\max_{\omega \in [0,\ \pi/h]} |S(e^{j\omega h})| = \sup_{w \in \ell_2} \frac{\|u\|_2}{\|w\|_2} \tag{14}$$

For a finite length data, the lower bound of the ℓ_2 gain can be estimated by

$$\max_{\omega \in [0,\ \pi/h]} |S(e^{j\omega h})| > \frac{\|\pi_q u\|_2}{\|\pi_q w\|_2} \tag{15}$$

By the way, a virtual disturbance is represented by using a given plant response data $u,\ y$ as

$$w = u + K_P y + K_I y_I + K_D y_D \tag{16}$$

where

$$y_I = \frac{h}{z-1} y \tag{17}$$

$$y_D = \frac{z-1}{zh} y \tag{18}$$

Therefore, from (15) and (16), the next value

$$\frac{\|\pi_q u\|_2}{\|\pi_q u + K_P \pi_q y + K_I \pi_q y_I + K_D \pi_q y_D\|_2}$$

can be used for an estimate of the ℓ_2 gain of the sensitivity function. In the next section, we will explain two algorithms for the calculation of the ℓ_2 gain from a given response data.

IV. ℓ_2 GAIN ESTIMATION ALGORITHMS

We will explain two algorithms that have been examined in [15].

A. Algorithm Using Bandpass Filter

In order to estimate the gain $|S(e^{j\omega_k h})|$ at sampling frequencies $\omega_k,\ k = 1, 2, 3, \cdots, n_\omega$ by using (15), we have proposed a method of filtering the plant responses by using a filter bank, i.e. many bandpass filters $F^k(z),\ k = 1, 2, 3, \cdots, n_\omega$. The bandpass filter $F^k(z)$ is given by discretizing the next continuous time transfer function with the sampling time h and a zero-order hold. α is the parameter for the tuning of the bandwidth and also the decay rate of the step response of the filter.

$$\tilde{F}^k(s) = \hat{\phi}(s/\omega_k),\ \hat{\phi}(s) = \left(\frac{2\alpha s}{(s+\alpha)^2 + 1} \right)^4 \tag{19}$$

Algorithm 1 First unbias the data by $u_i - u_0, y_i - y_0$ for $i > 0$. Then, obtain $u^k, y^k,\ y_I^k, y_D^k$ by filtering $u,\ y,\ y_I,\ y_D$ with the bandpass filters F^k for $k = 1, 2, 3, \cdots, n_\omega$, respectively. Next, estimate $|S(e^{j\omega h})|$ at the sampling frequencies by

$$\gamma_k = \frac{\|\pi_q u^k\|_2}{\|\pi_q u^k + K_P \pi_q y^k + K_I \pi_q y_I^k + K_D \pi_q y_D^k\|_2} \\ , k = 1, 2, \cdots, n_\omega \tag{20}$$

Lastly, estimate the ℓ_2 gain by

$$\gamma_a = \max_k \gamma_k \tag{21}$$

The next theorem is satisfied for infinite signals.

Theorem 1: Denote the bandwidth of $F^k(z)$ as $\Omega = [\underline{\omega},\ \overline{\omega}]$, and denote the signal obtained by filtering $u,\ y$ with $F^k(z)$ as $u^k,\ w^k$, respectively. Then, the next inequalities hold.

$$\min_{\omega \in \Omega} |S(e^{j\omega h})|(1-\delta_1)^{0.5} \leq \frac{\|u^k\|_2}{\|w^k\|_2} \\ \leq \max_{\omega \in \Omega} |S(e^{j\omega h})| \left\{1 + \delta_2\right\}^{0.5} \tag{22}$$

$$\delta_1 = \frac{h}{2\pi} \frac{\int_{\omega \notin \Omega} |F(e^{j\omega h}) w(e^{j\omega h})|^2 d\omega}{\|Fw\|_2^2}$$

$$\delta_2 = \left(1 + \frac{\max_{\omega \notin \Omega} |S(e^{j\omega h})|^2}{\max_{\omega \in \Omega} |S(e^{j\omega h})|^2} \right) \delta_1$$

This theorem can be proved by using Parseval's theorem. The proof is omitted.

Theorem 1 implies that the gain at a sampling frequency can be estimated more accurately as δ_1 is smaller and the change of $|S(e^{j\omega h})|$ in Ω is smaller.

Theorem 2: [15]. $\gamma_a \leq \gamma^*$ holds for the ℓ_2 gain given by

$$\gamma^* = \max_{\omega \in [0,\ \pi/h]} |S(e^{j\omega h})| \tag{23}$$

Since (22) is satisfied for infinite length data and (20) is calculated for finite length data, the estimated value by (20) is different from the ℓ_2 gain of Theorem 1. In order to make the value of (20) closer to the ℓ_2 gain of Theorem 1, we have proposed a method of setting α adequately. Since the filter has four zeros at $z = 1$, the amplitude of filtered outputs converge to zero for step or ramp signals. For these signals, the amplitude of filtered outputs sufficiently small at the end of

the finite length data, i.e. at q step by setting α appropriately. From numerical experiments, we have the next rule [15]. For $\omega = \omega_k$ and $M = qh\omega_k/(2\pi)$,

1) if $M > 20$, set $\alpha = 1/20$
2) if $20 \geq M \geq 1$, set $\alpha = 1/M$
3) if $1 < M$, set $\alpha = 1$.

B. Algorithm Based on Extension Theorem

Define the lower Toeplitz matrix $U \in R^{q\times q}$ for a sequence $\pi_q u = \{u_0, u_1, \cdots, u_{q-1}\}$ by

$$U = \begin{bmatrix} u_0 & 0 & \cdots & 0 \\ u_1 & u_0 & \cdots & 0 \\ \vdots & \vdots & \ddots & \vdots \\ u_{q-1} & u_{q-2} & \cdots & u_0 \end{bmatrix} \tag{24}$$

Lemma 1: [14] Let the operator S be stable, causal, and linear time-invariant, and suppose that a set of response data $\pi_q w, \pi_q u$ are given. Then, if

$$U^T U \leq \gamma^2 W^T W \tag{25}$$

is not satisfied, the ℓ_2 gain of S is greater than γ, where W,U are the Toeplitz matrices for $\pi_q w, \pi_q u$, respectively.

The next theorem is derived immediately from Lemma 1.

Theorem 3: Denote the Toeplitz matrices for $\pi_q y_D,\ \pi_q y_I$ as Y_D, Y_I. Let γ_b be the minimum value of γ that satisfies the next inequality for a fixed PID gain $f = [K_P, K_I, K_D]$, then γ_b gives a lower bound of the ℓ_2 gain of $S(z)$.

$$\begin{aligned} &U^T U \leq \gamma^2 W^T W \\ &W = U + (K_P Y + K_I Y_I + K_D Y_D) \end{aligned} \tag{26}$$

Algorithm 2 Calculate the singular value decompositions of $U,\ W$ as $U = U_U \Sigma_U V_U^T,\ W = U_W \Sigma_W V_W^T$, respectively, where Σ_W is positive definite. Calculate γ_b by

$$\gamma_b = \bar{\sigma}(\Sigma_U V_U^T V_W \Sigma_W^{-1}) \tag{27}$$

Theorem 4: [15] The next inequalities are satisfied.

$$\gamma_a \leq \gamma_b \leq \gamma^* \tag{28}$$

Since the extension theorem gives a necessary and sufficient condition for the existence of a time-invariant system that satisfies the plant response data and the ℓ_2 gain constraint, γ_b gives the most accurate value that can be estimated from the finite length data. For this reason, we have compared our method with it in our previous study, and we will also compare them for the visualization problem in this paper.

γ_b is useful as a benchmark to compare the accuracy with other methods. However, it should be carefully used for practical applications. This is because γ_b is very sensitive to the noise of the responses, and the computation time increases very rapidly as the data length q increases.

C. Visualization of Intersection of Two Sets

In this subsection, let us consider the visualization of the intersection of $\mathcal{F}_S$ and $\mathcal{F}_T$. We will consider this problem under the assumption that the volume data have already been calculated. Namely, for the grid points f, estimates of the maximum sensitivity $\hat{\gamma}_S(f)$ and the maximum complementary sensitivity $\hat{\gamma}_T(f)$ have already been given. Then, we may visualize a set of f that satisfies

$$\hat{\gamma}_S(f) < \gamma_S \tag{29}$$
$$\hat{\gamma}_T(f) < \gamma_T \tag{30}$$

simultaneously.

Our solution is to make a new volume data at each grid point f for given γ_S and γ_T by

$$\hat{\gamma}_{ST}(f) = \sqrt[n]{\left(\frac{\hat{\gamma}_S(f)}{\gamma_S}\right)^n + \left(\frac{\hat{\gamma}_T(f)}{\gamma_T}\right)^n} \tag{31}$$

where n is a large natural number and we use $n = 10$ in numerical examples.

As is obvious from the property of p-norm, if

$$\hat{\gamma}_{ST}(f) < 1 \tag{32}$$

, (29) and (30) are satisfied. This implies that the level set for the volume data $\hat{\gamma}_{ST}(f)$ with $\gamma_{ST} = 1$ is contained by the intersection of the level sets for the volume data $\hat{\gamma}_S(f)$ with γ_S and $\hat{\gamma}_T(f)$ with γ_T.

The effort for the computation of (31) from $\hat{\gamma}_S(f)$ and $\hat{\gamma}_T(f)$ is very small. Thus, we have the next algorithm.

step1	Obtain one shot plant response u and y. Set the grid points in the PID gain space.
step2	Make the volume data by computing $\hat{\gamma}_S(f)$,$\hat{\gamma}_T(f)$ for u, y for all the grid points.
step3	Set $\gamma_S,\ \gamma_T$, and make the volume data by computing $\hat{\gamma}_{ST}(f)$
step4	Visualize the level set $\hat{\gamma}_{ST}(f) = 1$.
step5	Find f for which K_I is maximized inside the level set. Go to Step 3 for another values of γ_S, γ_T.

V. NUMERICAL EXPERIMENTS

The plant transfer function $P(z)$ is given by discretizing $\tilde{P}(s)$ of (33) with sampling period $h = 0.05$[s] and zero-order hold.

$$\tilde{P}(s) = \frac{1}{s^2 + s + 1} \frac{120 - 60s + 10s^2 - s^3}{120 + 60s + 10s^2 + s^3} \tag{33}$$

First, we obtain a response of the plant $P(z)$ to the unit step input $u(t) = 1$ by simulation. The response $y(t),\ t = 0.05(i-1),\ \ i = 1,\ 2,\ \cdots, 400$ is shown in Fig. 3. These u and y are used for visualization.

Next, we make a volume data by Algorithm 1. Sample frequencies are selected as logarithmically equally spaced $n_\omega = 200$ points from the interval $[10^{-2}, 10^2]$[rad/s]. The grid points are selected for each axis $K_P,\ K_I,\ K_D$ with the same intervals of 0.05, and the number of grid points becomes $20 \times 12 \times 20 = 4800$. Thus, γ_a is calculated following (20) and (21) for the 4800 grid points by using the above data u and

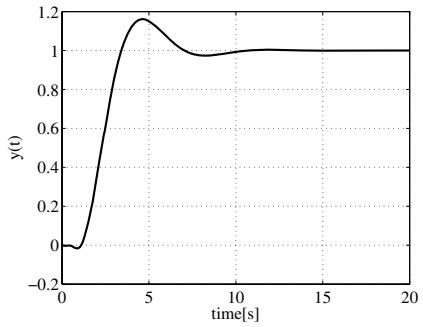

Fig. 3. A plant response data used for the ℓ_2 gain estimation

y. The unfalsified set is drawn by using volume visualization of MATLAB as shown in Fig. 4. This graphical object can be rotated, and it expands by increasing γ_S, and it shrinks by decreasing γ_S. These can be executed in real time.

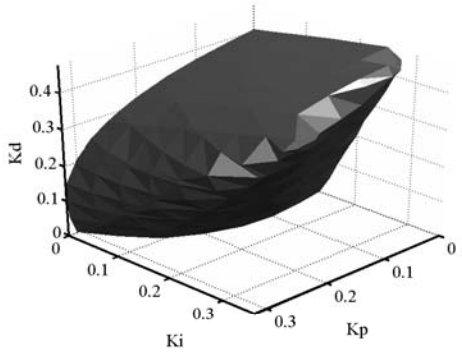

Fig. 4. PID gain set unfalsified by the filtering method

Similarly, we make a volume data by Algorithm 2. γ_b is calculated following (27) for the 4800 grid points by using the same data u and y. Further, we make a volume data for γ^* by calculating the H_∞ norm of the sensitivity function by using the mathematical model $P(z)$. These three graphical representations look very similar to each other.

Therefore, we compare the computation errors $e_a,\ e_b[\%]$ of γ_a and γ_b from the true value γ^* by using

$$e_a = \left| \frac{\gamma^* - \gamma_a}{\gamma^*} \right| \times 100 \tag{34}$$

$$e_b = \left| \frac{\gamma^* - \gamma_b}{\gamma^*} \right| \times 100 \tag{35}$$

The average and maximum values of the errors are calculated for the grid points inside the level set determined by the fixed values of γ^*, and the results are summarized in Table I. We may say from Table I that the two algorithms are similar in computational accuracy.

TABLE I. AVERAGE ERROR [MAXIMUM ERROR] [%]

γ	1.3	1.5	2
Bandpass	3.75[10.95]	6.03[17.63]	10.48[29.03]
Extension	3.60[10.95]	5.82[20.79]	10.03[29.63]

Next, compare the two algorithms in computational effort. Our computation environment is as follows. OS:Windows 7 Professional 64bit, CPU:Intel Corei7 970, 3.2[GHz], memory:24576MB, MATLAB2011a and Parallel Computing Toolbox.

The computation time is measured for the time intervals $T = 20,\ 30,\ 40$, which correspond to the data length $400,\ 600,\ 800$, respectively. The response data are the same as those of Fig. 3 except for the data length. CPU time that is used for the calculation of the volume data are listed in Table II. We used the command of Parallel Computing Toolbox "parfor" for parallel computation. The results of the computation time without parallel computation are listed in Table III. By the way, if the H_∞ norm of the sensitivity function is computed by using the command "norm" for $P(z)$, the computation time is 45.88[s].

TABLE II. CALCULATION TIME FOR VOLUME DATA GENERATION WITH PARALLEL COMPUTATION

T[s]	20[s]	30[s]	40[s]
q	400	600	800
Bandpass	12.49[s]	12.57[s]	12.49[s]
Extension	366.37[s]	1157.91[s]	3323.38[s]

TABLE III. CALCULATION TIME FOR VOLUME DATA GENERATION WITHOUT PARALLEL COMPUTATION

T[s]	20[s]	30[s]	40[s]
n	400	600	800
Bandpass	22.427[s]	22.445[s]	22.836[s]
Extension	838.51[s]	2160.16[s]	4385.20[s]

The two algorithms are similar in accuracy, but completely different in computation time. Since the computation time by Algorithm 2 is about 55 minutes for $q = 800$ and this data length is normal, Algorithm 2 is not applicable to practical problems. On the other hand, computation time by Algorithm 1 does not increase though the data length increases, and it is about 13 seconds for all the q's. Algorithm 1 is considered to be practical.

VI. DESIGN EXAMPLE

Let us consider a benchmark problem of a boiler model[16], which is based on the nonlinear model in [17] but the mathematical model is not open. We will design a PID controller from a plant response. The input of the plant u is the fuel flow, and the output of the plant y is the steam pressure. Other control loops are closed with PID controllers adequately. The controller $K(z)$ is the next PID controller with sampling period $h = 10$[s].

$$K(z) = K_P + K_I \frac{10z^{-1}}{1 - z^{-1}} + K_D \frac{1 - z^{-1}}{10(1.01 - 0.01z^{-1})} \tag{36}$$

First, a step test input is given at the plant input of the closed-loop system where the PID gains are $K_P = 1, K_I = 0.01, K_D = 0$. The plant responses u, y are shown in Fig. 5 and Fig. 6.

The sampling frequencies are logarithmically equally spaced 100 points in the interval $[10^{-3},\ \log_{10}(0.314)]$[rad/s].

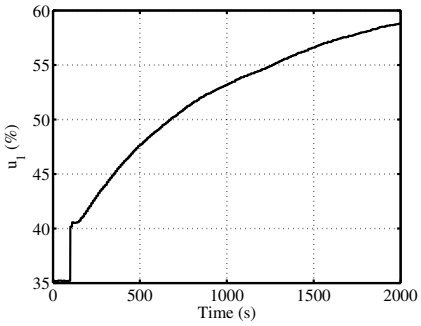

Fig. 5. Plant input u used for design

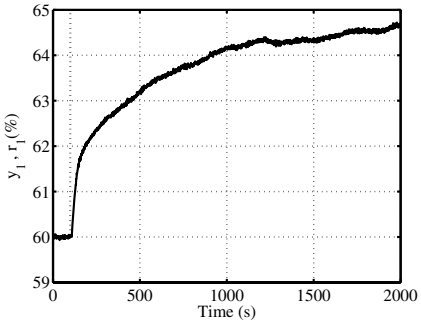

Fig. 6. Plant output $y$used for design

Grid points are selected at the intervals of 0.1, 0.005, 0.5 for K_P, K_I, K_D in the intervals $[0,\ 4]$, $[0,\ 0.15]$, $[0,\ 25]$, respectively. Volume data $\hat{\gamma}_S(f), \hat{\gamma}_T(f)$ are computed for the grid points, where the computation time is 33.407[s]. The set that satisfies these simultaneously can be visualized by using the volume data calculated by (31) with $n = 10$ for a given γ_S, γ_T in real time. Fig. 7 shows the unfalsified set for $\gamma_S = 2, \gamma_T = 1$.

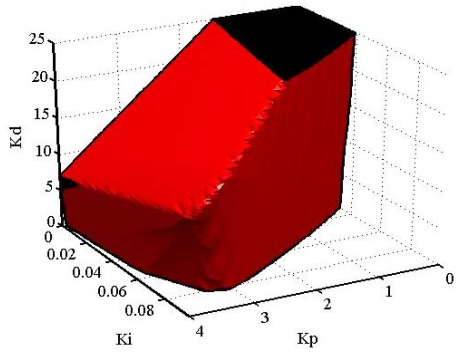

Fig. 7. $\hat{\gamma}_{ST}(f)$ in the PID gain space

From this figure, we can globally find a point $K_P = 3.9, K_I = 0.11, K_D = 14$ for which K_I is almost maximized in the unfalsified set. On the other hand, our numerical optimization method gives a local solution $K_P = 3.97, K_I = 0.106, K_D = 13.6$, and these gains almost agree to each other.

VII. CONCLUSIONS

In this paper, we have proposed to apply volume rendering to the visualization of the unfalsified PID gain set in the 3D space. We have shown numerically that computational effort to make the volume data is not so heavy by our ℓ_2 gain estimation method. We have made it certain that our method can be practical. In the examples, we have tested the parallel computation by using "parfor" of MATLAB, and the computation time can be made much shorter by using GPU computation. Volume data visualization and parallel computation depend on the recent development of computer technology. It is expected that the computer performance will be further strengthened in this direction. We will examine the computation time on GPU.

ACKNOWLEDGMENT

The authors would like to thank Mr. Kohei Masuda for numerical experiments.

REFERENCES

[1] H. Hjalmarsson, Iterative feedback tuning: an overview, *International Journal of Adaptive Control and Signal Processing*, vol. 16, 2002, pp. 373-395.

[2] M.C. Campi, A. Lecchini, and S. M. Savaresi, Virtual reference feedback tuning: a direct method for the design of feedback controllers, *Automatica*, vol. 38, 2002, pp. 1337-1346.

[3] K. van Heusden, A. Karimi, and D. Bonvin, Data-driven controller tuning with integrated stability constraint, *47th IEEE Conference on Decision and Control*, Cancum, Mexico, 2008, pp. 2612-2617.

[4] O. Kaneko, M. Miyachi, and T. Fujii, Simultaneous updating of a model and a controller based on the data-driven fictitious controller, *47th IEEE Conference on Decision and Control*, Cancum, Mexico, 2008, pp. 1358-1363.

[5] M. Saeki, Model-free PID controller optimization for loop-shaping, *Proc. of the 17th World IFAC Congress*, 2008, pp. 4958-4962.

[6] M. Saeki and Y. Sugitani, Comparison of data-driven loop-shaping method, VRFT, and E-FRIT, *Proc. of SICE 10th Annual Conference on Control Systems*, Kumamoto, Japan, 2010 (in Japanese).

[7] L. Campestrini, D.Eckhard, M.Gevers, A.S. Bazanella, Virtual reference feedback tuning for non-minimum phase plants, *Automatica*, vol. 47, 2011, pp. 1778-1784.

[8] S. Skogestad and I. Postlethwaite, Multivariable Feedback Control: Analysis and Design, John Wiley & Sons, 1996.

[9] M.G. Safonov and Y.C. Tsao., The unfalsified control concept and learning, *IEEE Transactions on Automatic Control*, vol. 42, pp. 843-847, 1997.

[10] M. Stefanovic and M.G. Safonov., Safe adaptive control, Springer-Verlag London Limited, Lecture notes in control and information sciences 405, 2011.

[11] M. Saeki and R. Kishi, A data-driven PID control design by linear programming for stable plants, *Proc. of the 18th World IFAC Congress*, pp. 7420-7425, 2011.

[12] J. Ackermann, et al., Robust Control: The Parameter Space Approach, Springer-Verlag London Limited, 2002.

[13] K. Åström and and T. Hägglund, Advanced PID Control, ISA, 2006.

[14] K. Poolla, P.K. Khargonekar, et.al., A time-domain approach to model validation, *IEEE Trans. on Automatic Control*, 39-5, 951-959, 1994.

[15] M. Saeki, Gain characteristics estimation for data-driven control design and extension theorem, *American Control Conference*, 4028-4033, 2012.

[16] F. Morilla, Benchmark for PID control based on the boiler control problem (version: july 2011), http://www.dia.uned.es/ fmorilla/benchmarkPID2012/, 2011.

[17] G. Pellegrinetti and J. Bentsman, Nonlinear control oriented boiler modeling-A benchmark problem for controller design, *IEEE Transactions on Control Systems Technology*, vol. 4, pp. 57-64, 1999.